Electronic Supplementary Information (ESI)

Pushing the limit of synergy in SnTe-based thermoelectric materials leading to an ultra-low lattice thermal conductivity and enhanced ZT

Samuel Kimani Kihoi,[a] U. Sandhya Shenoy,[b] Joseph Ngugi Kahiu,[c] Hyunji Kim,[a] D. Krishna Bhat [d] and Ho Seong Lee* [a,c]

[a] School of Materials Science and Engineering, Kyungpook National University, 80 Daehak-ro, Buk-gu, Daegu, 41566, Republic of Korea

[b] Department of Materials Science and Engineering, Institute of Engineering and Technology, Srinivas University, Mukka -574146, Mangalore, Karnataka, India

[c] Department of Hydrogen and Renewable Energy, Kyungpook National University, 80 Daehak-ro, Buk-gu, Daegu, 41566, Republic of Korea

[d] Department of Chemistry, National Institute of Technology Karnataka, Surathkal, Srinivasnagar -575025, Mangalore, Karnataka, India

*hs.lee@knu.ac.kr

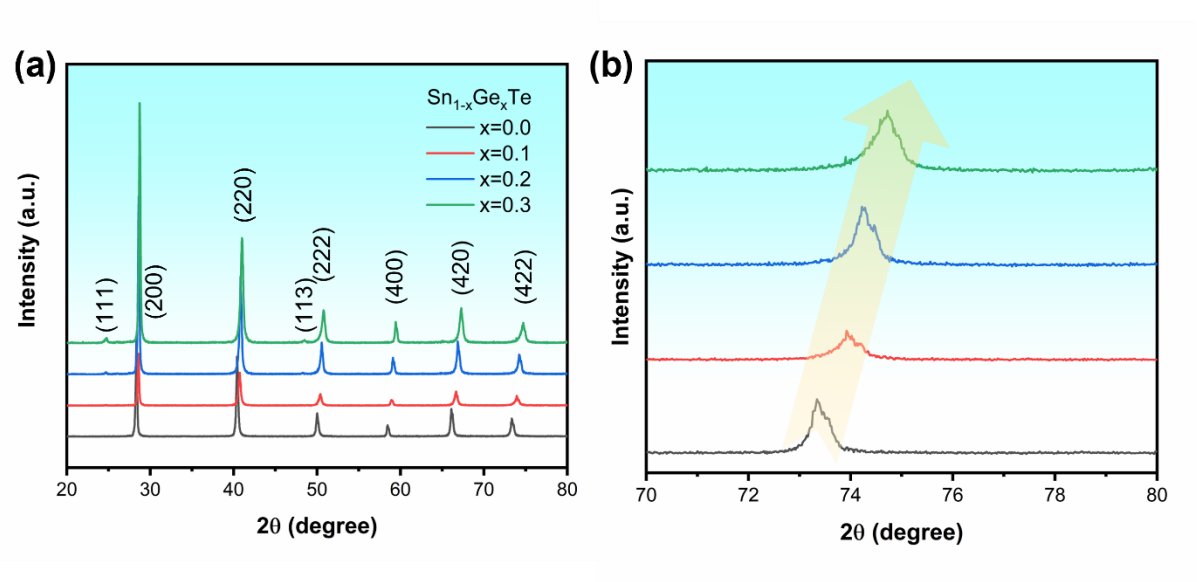

Fig. S1 (a) XRD patterns of the bulk $Sn_{1-x}Ge_xTe$ compositions and (b) peak shift at a high angle.

Table S1 Lattice parameter of the $Sn_{1-x}Ge_xTe$ compositions.

Composition (x)	**a (Å)**
0.0	6.317
0.1	6.273
0.2	6.252
0.3	6.219

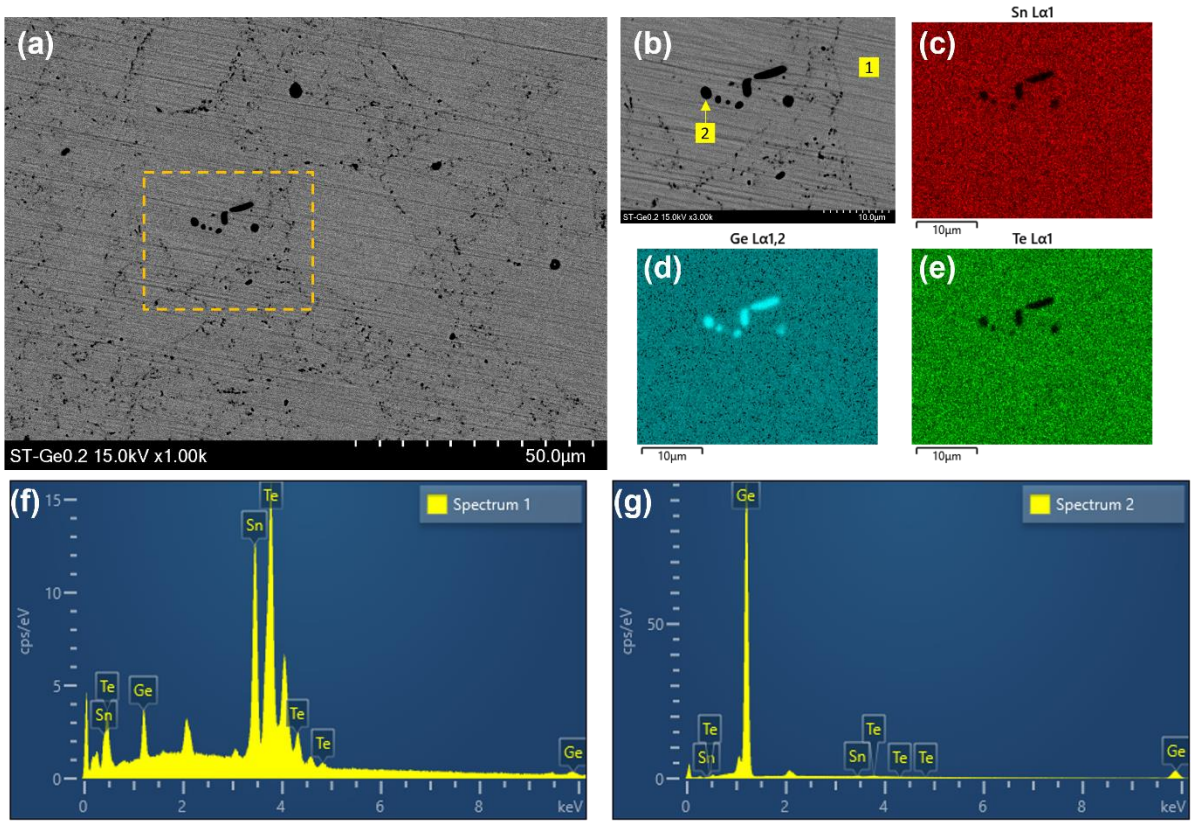

Fig. S2 (a) BSE image of the $Sn_{0.8}Ge_{0.2}Te$ composition, (b-e) corresponding EDS mapping and (f, g) point spectrum of points 1 and 2 in (b) respectively.

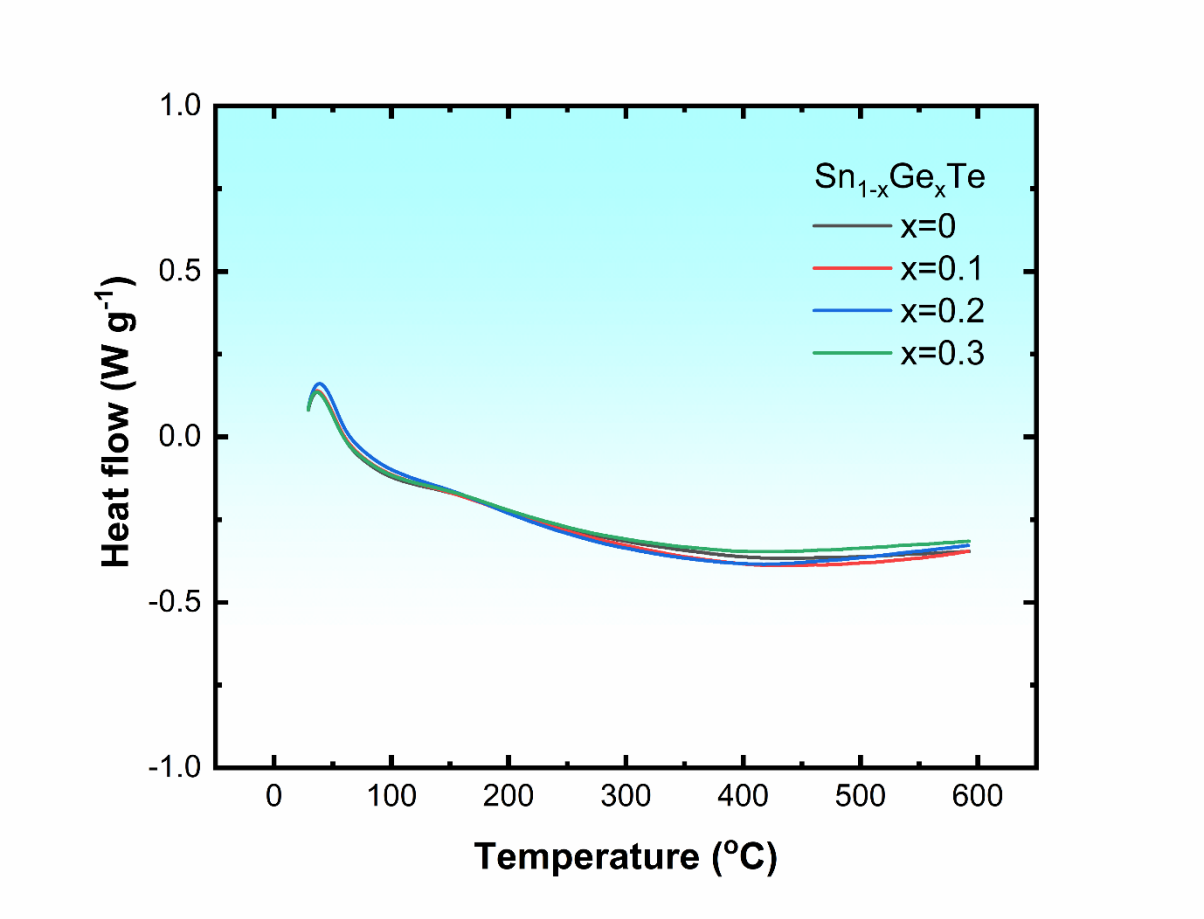

Fig. S3 DSC curves of the $Sn_{1-x}Ge_xTe$ compositions.

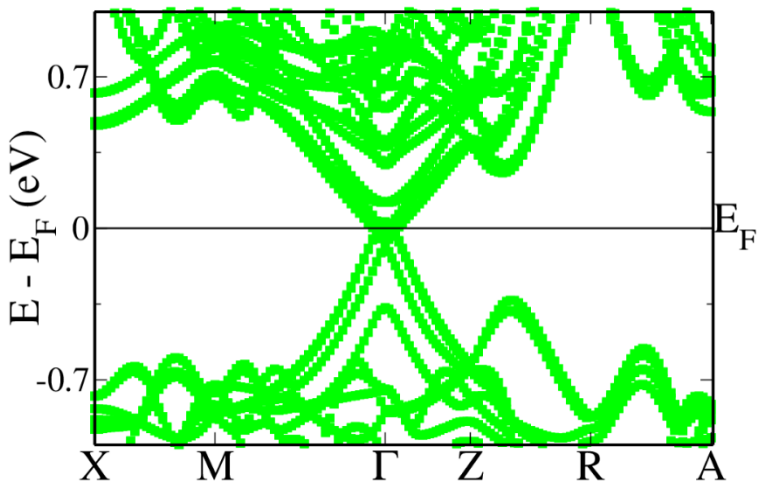

Fig. S4 Electronic structure of $Sn_{13}Ge_3Te_{16}$. Energies are shifted with respect to the Fermi level which is set to zero.

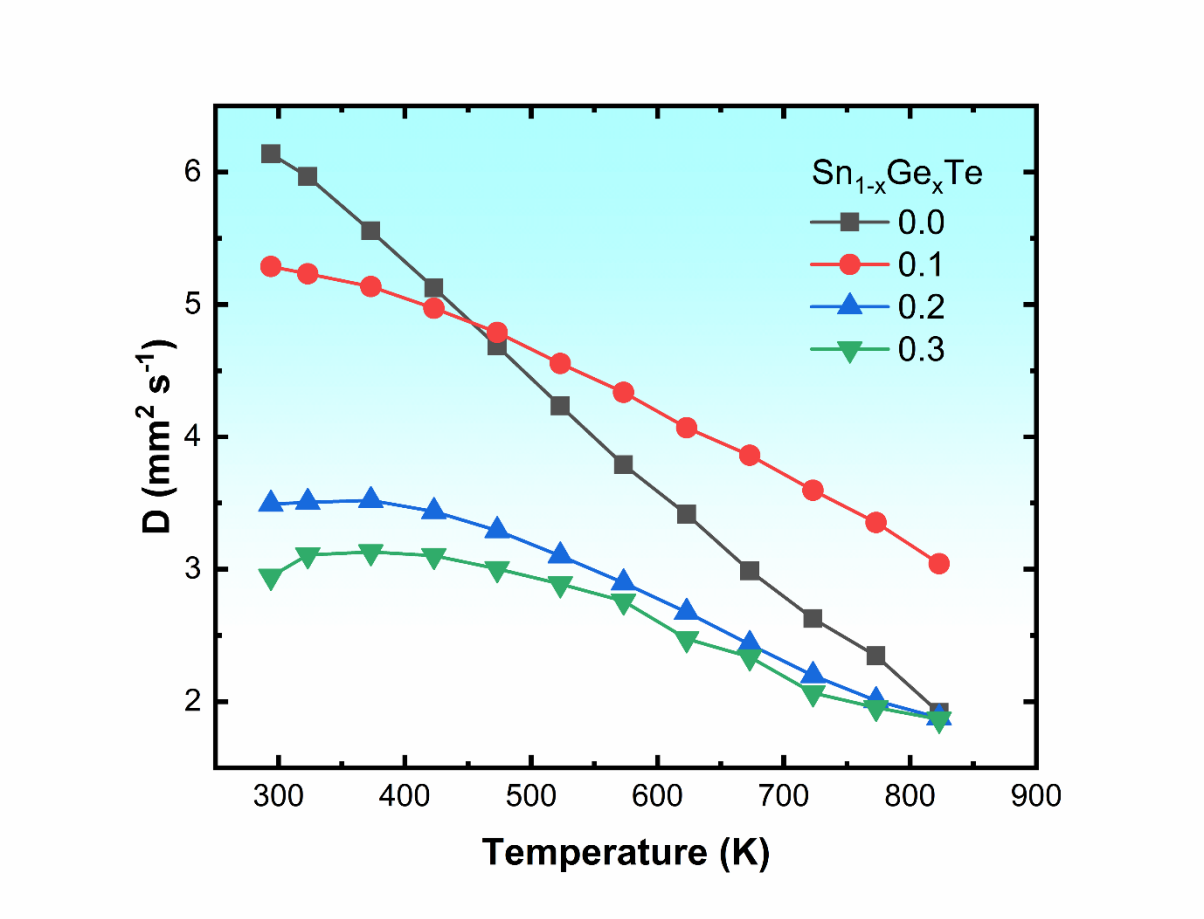

Fig. S5 Thermal diffusivity values $Sn_{1-x}Ge_xTe$ compositions.

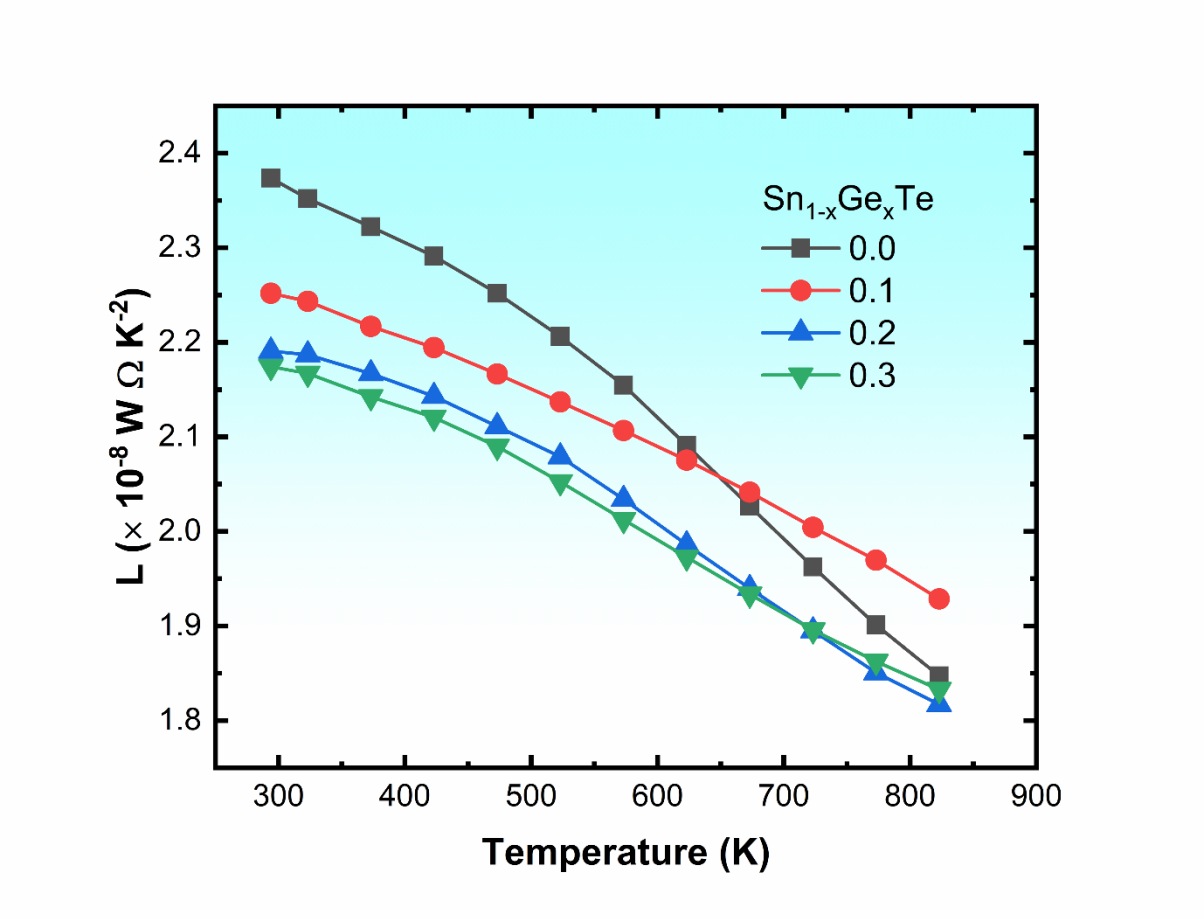

Fig. S6 Lorenz number for the $Sn_{1-x}Ge_xTe$ compositions.

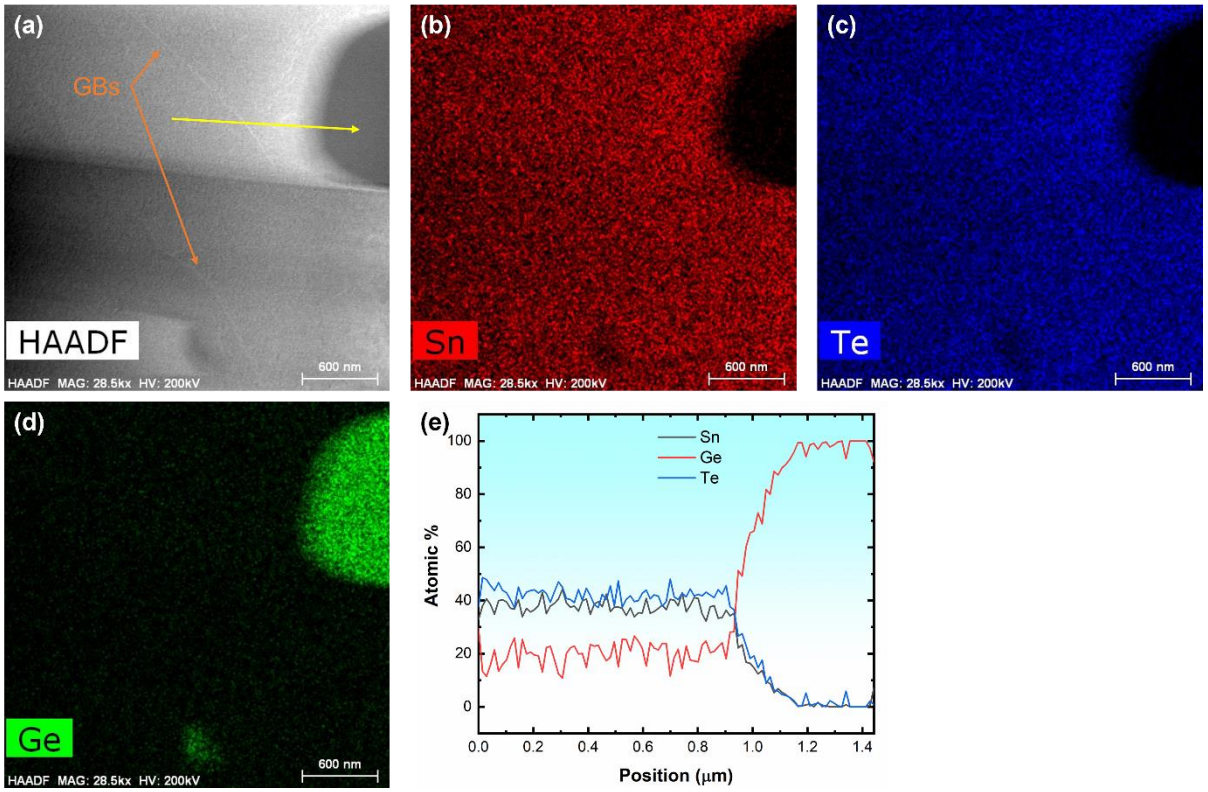

Fig. S7 (a) HAADF image, (b-d) corresponding EDS mapping and (e) line scan data along the yellow arrow in (a) of the $Sn_{0.8}Ge_{0.2}Te$ composition.

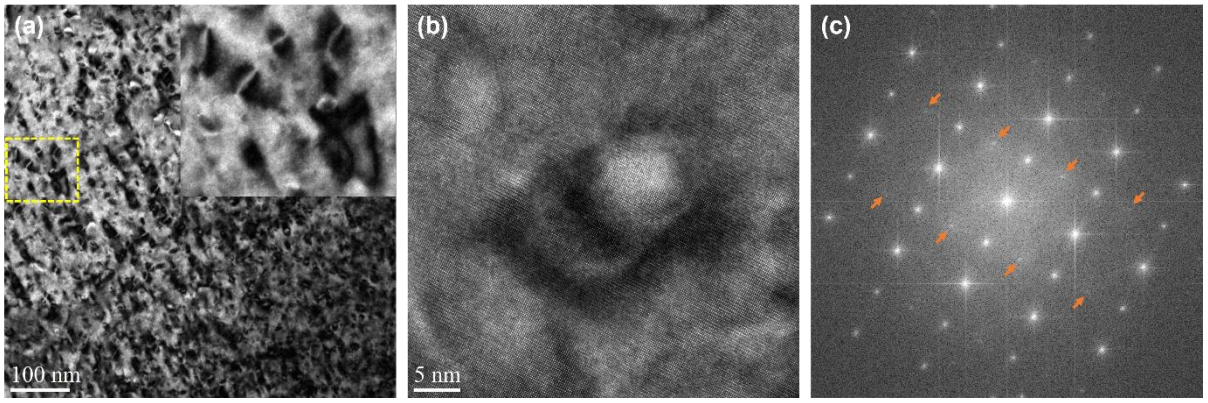

Fig. S8 (a) BF, (b) HRTEM and (c) SAED pattern of the $Sn_{0.8}Ge_{0.2}Te$ composition.

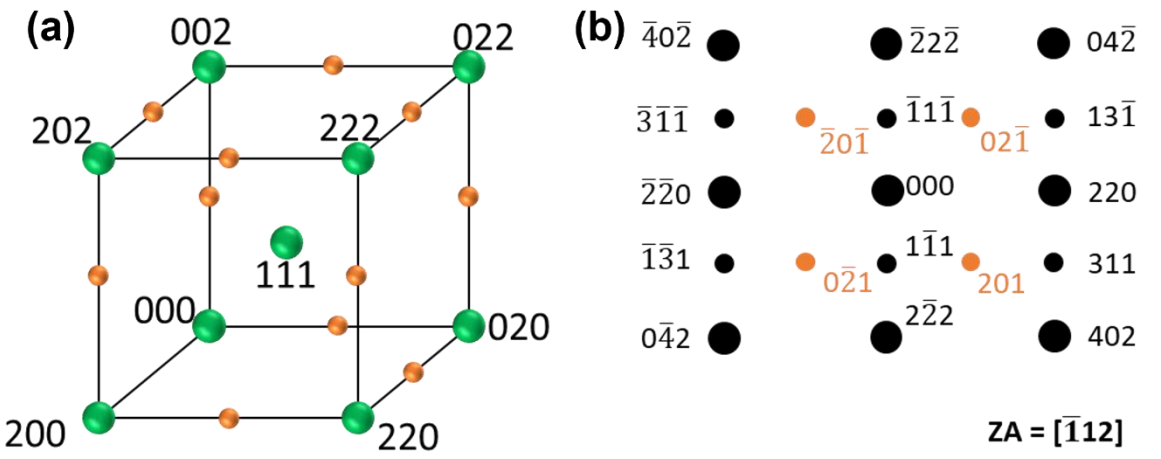

Fig. S9 Schematic representation of the ordered phase, (a) reciprocal lattice unit cell and (b) corresponding diffraction pattern along the [$\bar{1}$12] zone axis.

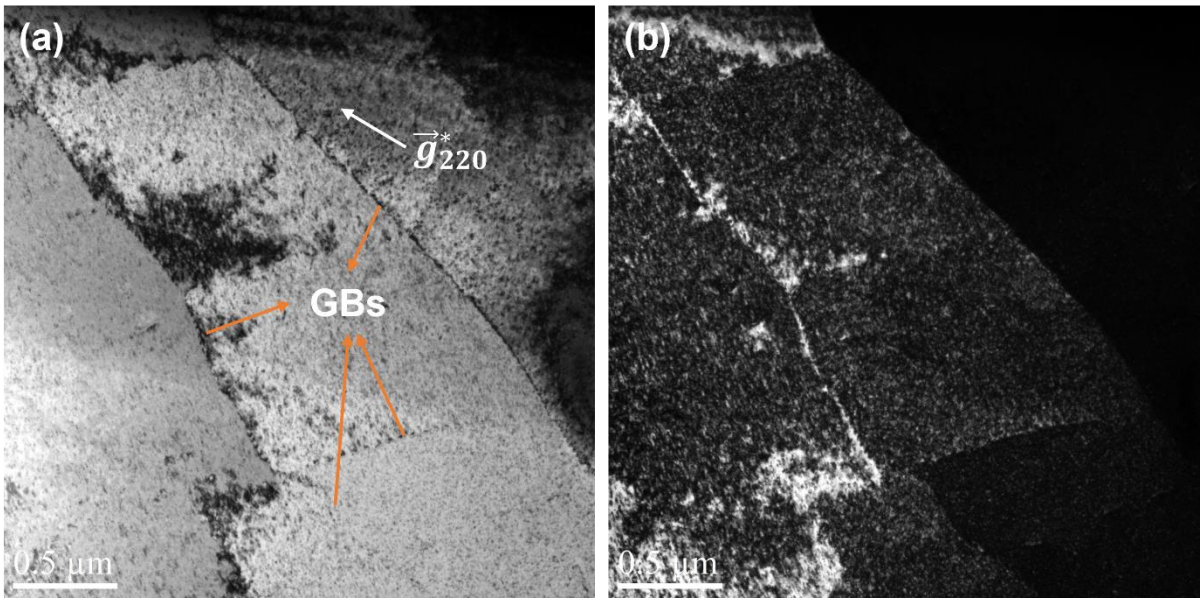

Fig. S10 Two beam (a) BF and (b) DF image of the $Sn_{0.8}Ge_{0.2}Te$ composition.

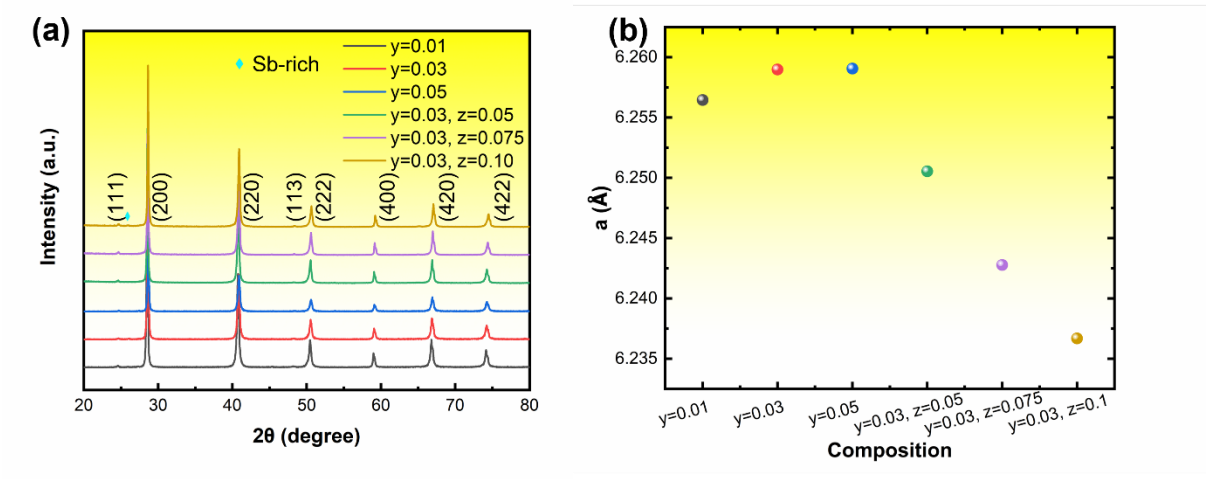

Fig. S11 (a) XRD patterns of the bulk $Sn_{0.8-y-z}Ge_{0.2}Bi_ySb_zTe$ compositions and (b) corresponding lattice parameter values.

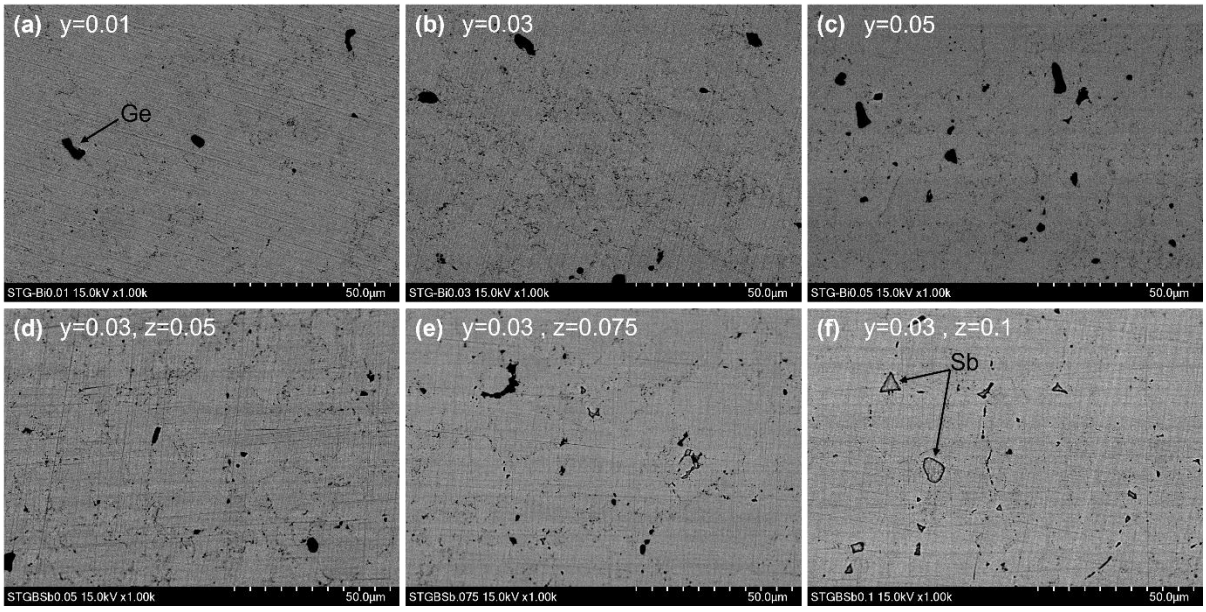

Fig. S12 BSE images of the $Sn_{0.8-y-z}Ge_{0.2}Bi_ySb_zTe$ compositions.

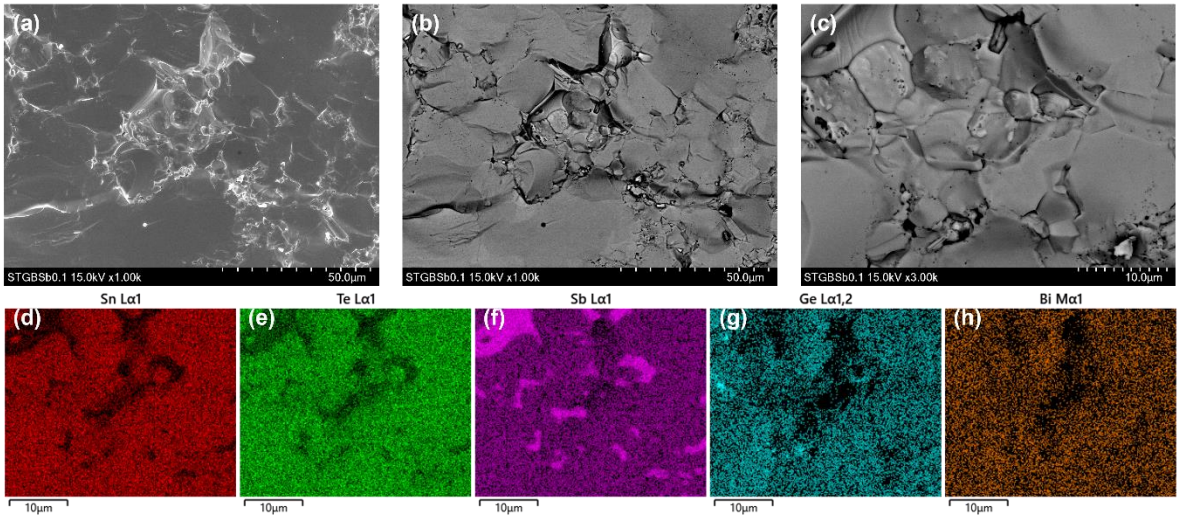

Fig. S13 Fracture analysis showing (a) SE, (b) BSE low magnification, (c) BSE high magnification and (d-h) corresponding EDS mapping of the $Sn_{0.67}Ge_{0.2}Bi_{0.03}Sb_{0.1}Te$ composition.

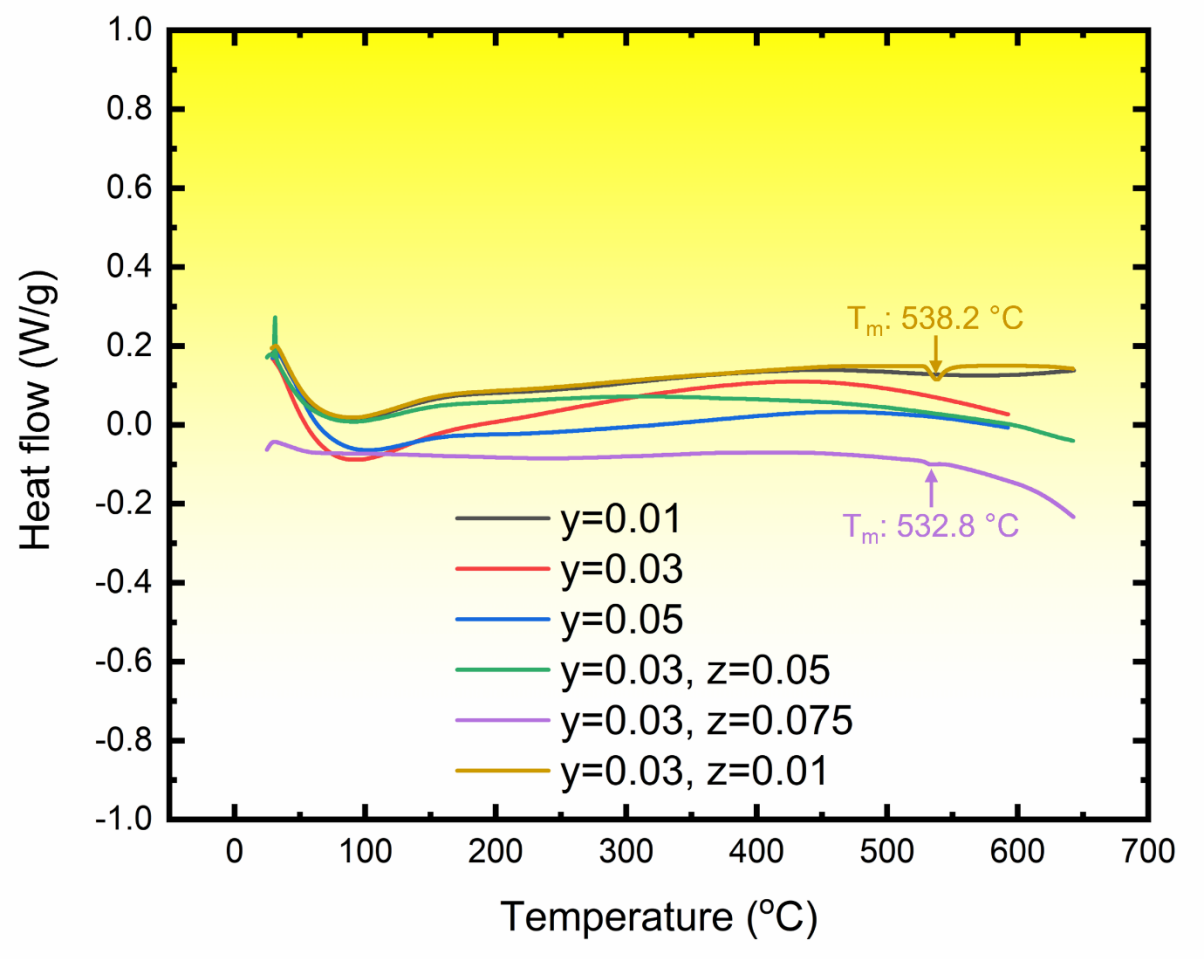

Fig. S14 DSC curves for the $Sn_{0.8-y-z}Ge_{0.2}Bi_ySb_zTe$ compositions.

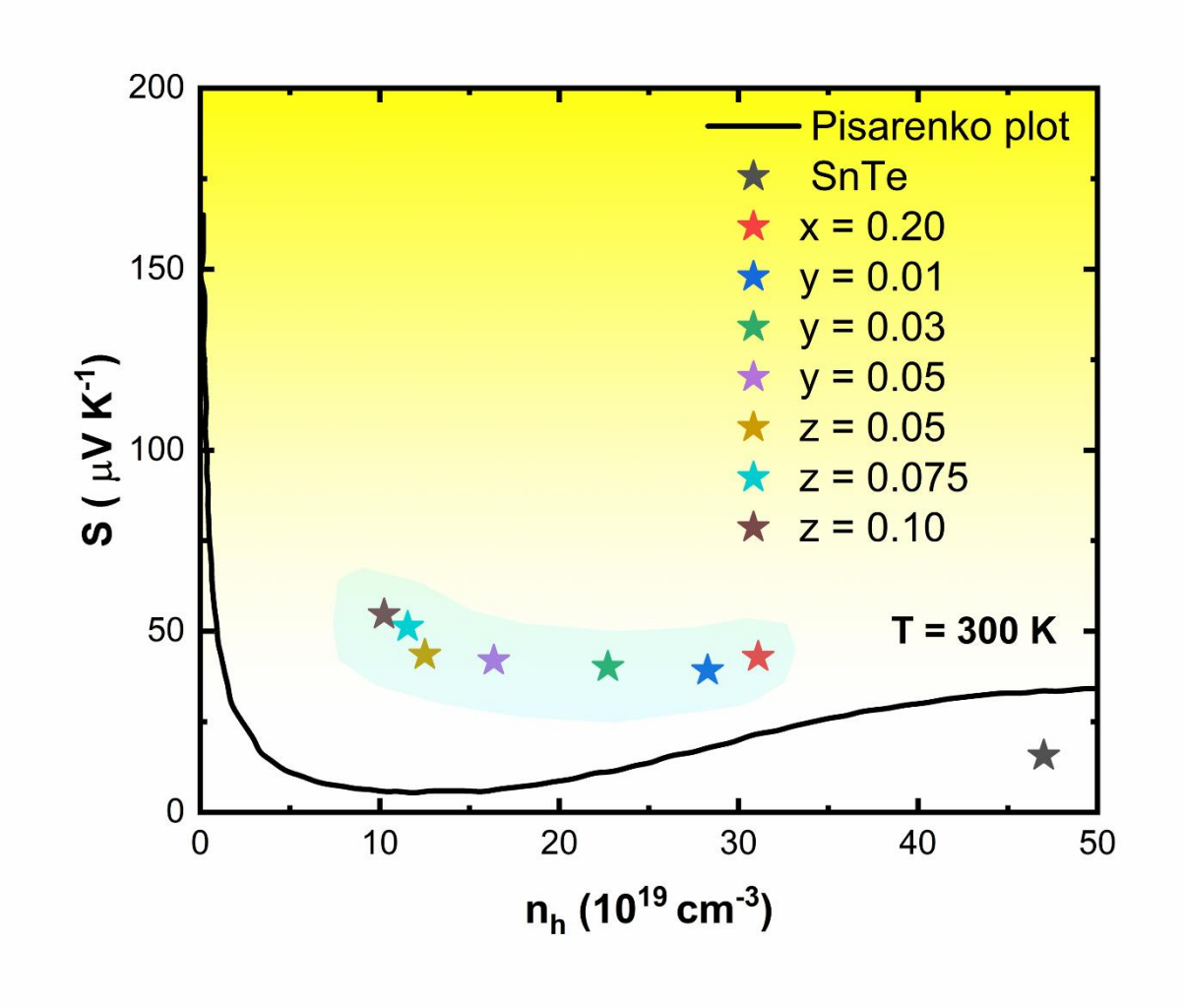

Fig. S15. Pisarenko plot comparing the experimental and theoretical Seebeck coefficient with carrier concentration. The solid line is the Pisarenko plot for SnTe adopted from Zhang et al.[1] at 300 K.

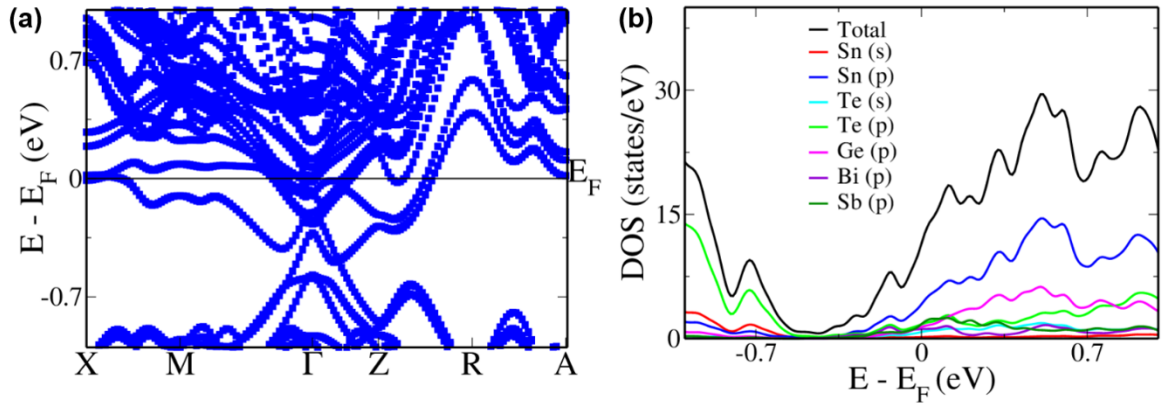

Fig. S16 Electronic structure and DOS of $Sn_{11}Ge_3BiSbTe_{16}$. Energies are shifted with respect to the Fermi level which is set to zero.

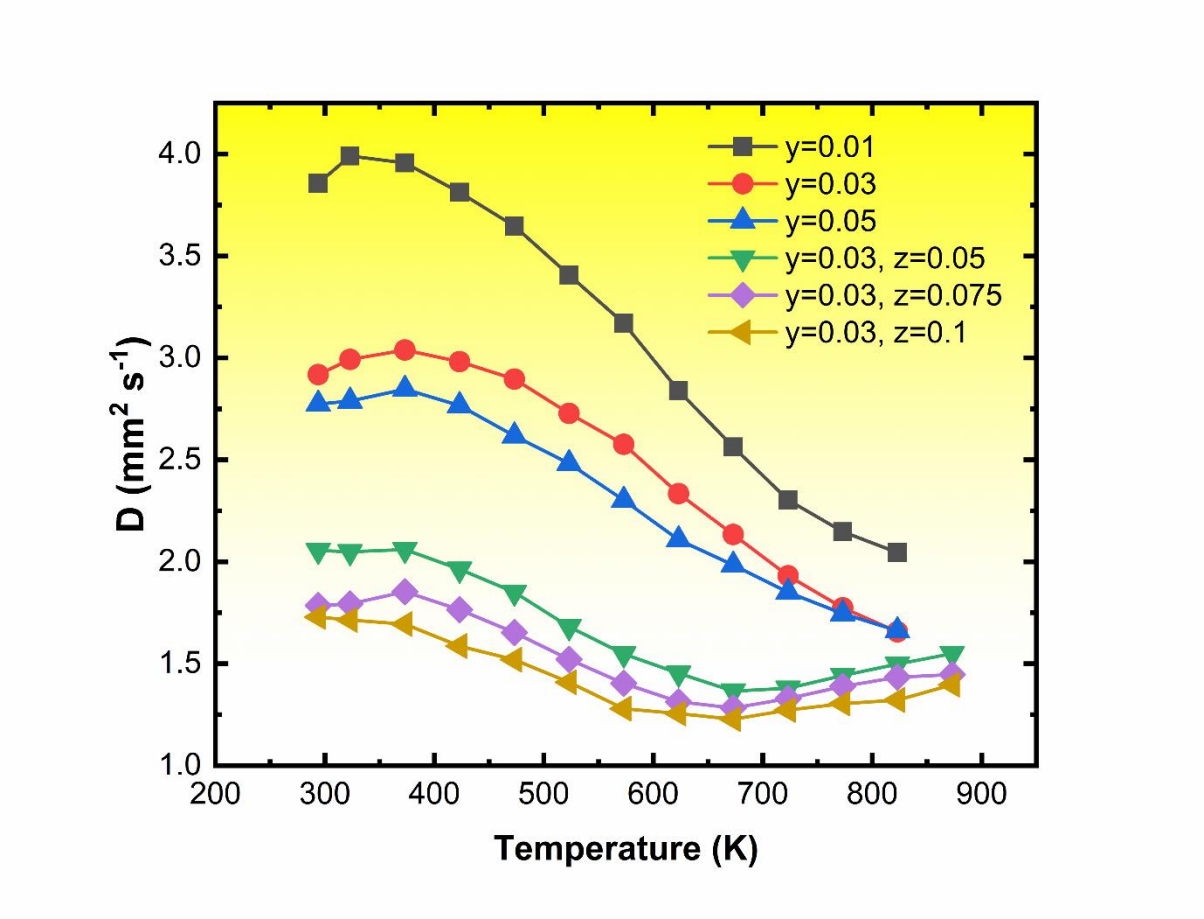

Fig. S17 Thermal diffusivity values for the $Sn_{0.8-y-z}Ge_{0.2}Bi_ySb_zTe$ compositions.

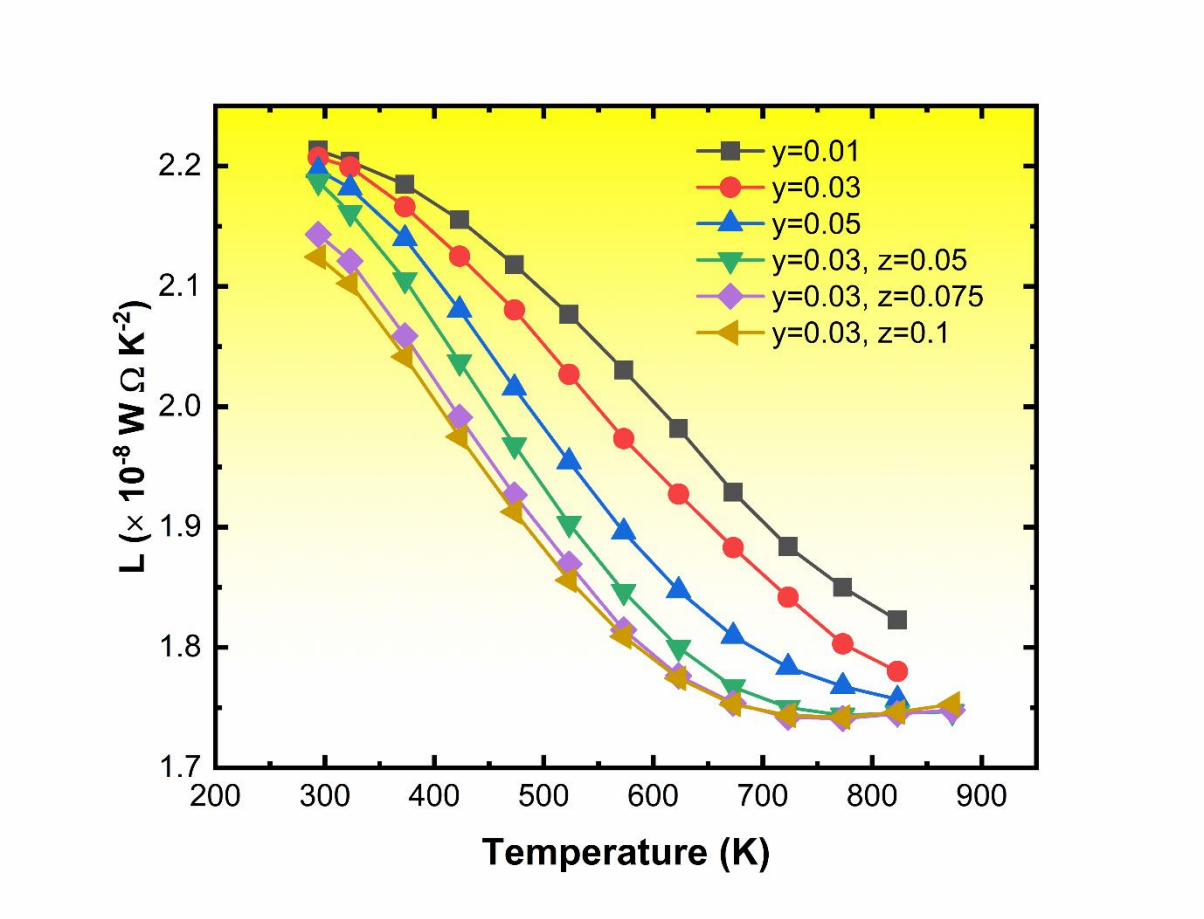

Fig. S18 Lorenz number for the $Sn_{0.8-y-z}Ge_{0.2}Bi_ySb_zTe$ compositions.

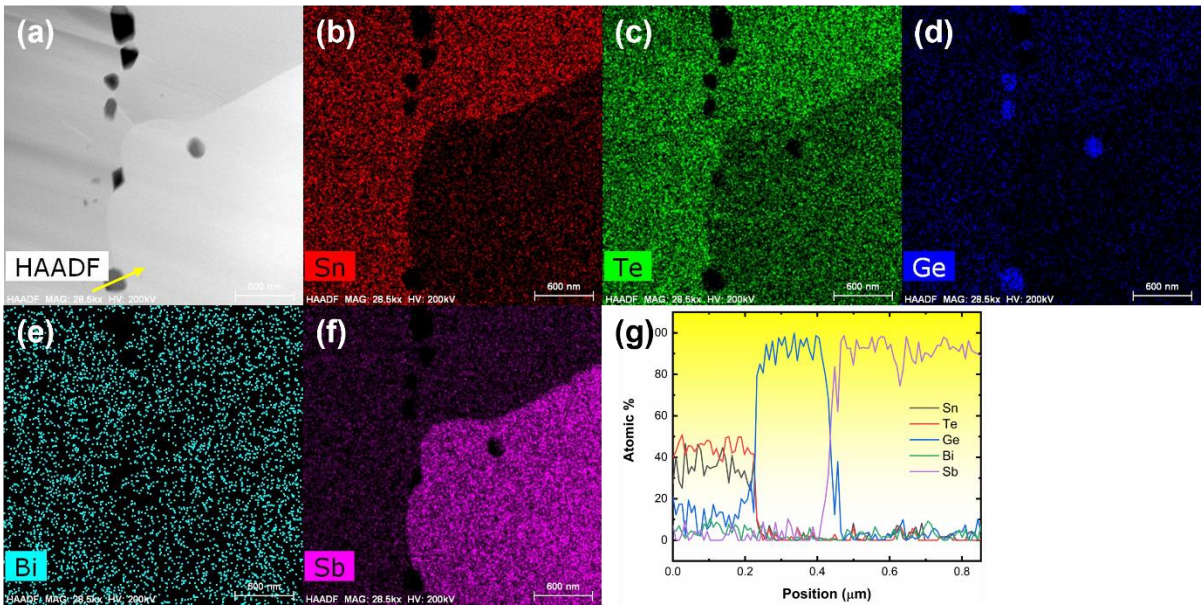

Fig. S19 (a) HAADF image, (b-f) corresponding EDS mapping and (e) line scan data along the yellow arrow in (a) of the $Sn_{0.67}Ge_{0.2}Bi_{0.03}Sb_{0.1}Te$ composition.

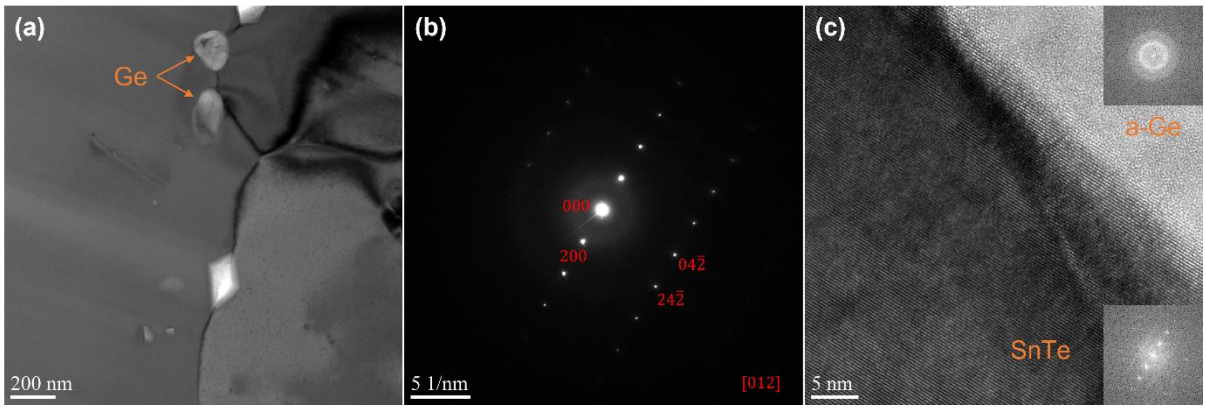

Fig. S20 (a) BF, (b) SAED pattern and (d) HRTEM image of the SnTe-Ge interface of the $Sn_{0.67}Ge_{0.2}Bi_{0.03}Sb_{0.1}Te$ composition.

Lattice thermal conductivity modelling

According to the Debye-Callaway model,[2] the lattice thermal conductivity is computed as shown in equation (S1).

$$\kappa_l = \frac{k_B}{2\pi^2 v}\left(\frac{k_B T}{\hbar}\right)^3 \int_0^{\theta_D/T} \tau_{tot}(x)\frac{x^4 \exp(x)}{[\exp(x)-1]^2}dx \quad \text{(S1)}$$

The integrand item of the equation above is the spectral lattice thermal conductivity which is calculated by equation (S2) below.[3–5]

$$\kappa_s = \frac{k_B}{2\pi^2 v}\left(\frac{k_B T}{\hbar}\right)^3 \tau_{tot}(x)\frac{x^4 \exp(x)}{[\exp(x)-1]^2}dx \quad \text{(S2)}$$

In the above equations, x is a dimensionless variable given by $x = \hbar\omega/k_B T$ where ω is the phonon frequency. θ_D is the Debye temperature which is calculated using $k_B\theta_D = \hbar v(6\pi^2 N)^{1/3}$ where N is the number of atoms per volume and v is the average sound velocity.[5–7] τ_{tot} is the combined relaxation time obtained after considering relaxation times due to the Umklapp process (U), Normal process (N), grain boundary scattering (GB), point defect scattering (PD), and nanoprecipitates scattering (NP). This is represented by the Matthiessen's rule below.

$$\tau_{tot}^{-1} = \tau_U^{-1} + \tau_N^{-1} + \tau_{GB}^{-1} + \tau_{PD}^{-1} + \tau_{NP}^{-1} \quad \text{(S3)}$$

Specific relaxation times are determined as described below.

Umklapp process:

$$\tau_U^{-1} = \frac{\hbar\gamma^2 x^2 T}{M v^2 \theta_D}\left(\frac{k_B T}{\hbar}\right)^2 exp\left(-\frac{\theta_D}{3T}\right) \quad \text{(S4)}$$

Where $k_B, \hbar, \gamma, T, and\ M$ are the Boltzmann constant, reduced Planck constant, Grüneisen parameter,[5,7] absolute temperature, and average atomic mass, respectively.

Normal process:

$$\tau_N^{-1} = \beta\tau_U^{-1} \quad \text{(S5)}$$

Where β is the ratio of Umklapp scattering to Normal phonon scattering.[5]

Grain boundary scattering:

$$\tau_{GB}^{-1} = \frac{v}{L} \tag{S6}$$

Where L is the average grain size taken from FESEM images.

Point defect scattering:

$$\tau_{PD}^{-1} = \left(\frac{k_B T}{\hbar}\right)^4 \frac{V_{atom}\Gamma}{4\pi v^3} x^4 \tag{S7}$$

Where V_{atom} and Γ are the average atomic volume and scattering parameter. The scattering parameter is calculated as:

$$\Gamma = x(1-x)\left[\left(\frac{\Delta M}{M}\right)^2 + \varepsilon\left(\frac{a_{disorder} - a_{pure}}{a_{pure}}\right)^2\right] \tag{S8}$$

Where x is the fractional concentration of the substituted elements, ΔM is the difference in atomic mass between pure and doped alloy, M is atomic mass of pure alloy, ε is the phenomenological parameter obtained from literature,[7] and a represent the lattice parameter of both pure and disordered alloy accordingly.

Nanoprecipitates scattering:

$$\tau^{-1} = v\left[(2\pi R^2)^{-1} + \left(\pi R^2 \frac{4}{9}\left(\frac{\Delta D}{D}\right)^2 \left(\frac{\omega R}{v}\right)^4\right)^{-1}\right]^{-1} N_p \tag{S9}$$

Where R is the average radius of the precipitates, ΔD difference is density between the matrix and precipitates, D is the density of the matrix and N_p is the number density of the precipitates.

Table S2 Input parameters of the lattice thermal conductivity modelling.

Input parameter	**Value**
Debye temperature, θ_D (K)	169.40
Average sound velocity, v (m s^{-1})	1800[5–7]
Grüneisen parameter, γ	2.2[5,7]

Average atomic mass, M (Kg)	2.05×10^{-25}
Ratio of Umklapp scattering to Normal phonon scattering, β	1.8[5]
Average grain size, L (m)	5.40×10^{-6}
Average atomic volume, V_{atom} (m^3)	3.17×10^{-29}
Phenomenological parameter, ε	83[7]
Average radius of precipitates, R (m)	9.1×10^{-8}
Number density of precipitates, N_p (m^{-3})	8.27×10^{18}

References

1 Q. Zhang, B. Liao, Y. Lan, K. Lukas, W. Liu, K. Esfarjani, C. Opeil, D. Broido, G. Chen and Z. Ren, *Proc. Natl. Acad. Sci.*, 2013, **110**, 13261–13266.

2 J. Callaway and H. C. Von Baeyer, *Phys. Rev.*, 1960, **120**, 1149–1154.

3 Q. Yang, T. Lyu, B. Nan, Y. Dong, J. Tie and G. Xu, *J. Eur. Ceram. Soc.*, 2022, **42**, 1001–1006.

4 R. Moshwan, W. Di Liu, X. L. Shi, Y. P. Wang, J. Zou and Z. G. Chen, *Nano Energy*, 2019, **65**, 104056.

5 T. Lyu, Q. Yang, F. Meng, J. He, A. Benton, C. Chronister, Z. Li and G. Xu, *Chem. Eng. J.*, 2021, **404**, 126925.

6 A. Banik, B. Vishal, S. Perumal, R. Datta and K. Biswas, *Energy Environ. Sci.*, 2016, **9**, 2011–2019.

7 F. Guo, B. Cui, Y. Liu, X. Meng, J. Cao, Y. Zhang, R. He, W. Liu, H. Wu, S. J. Pennycook, W. Cai and J. Sui, *Small*, 2018, **14**, 1802615.